ADVANCED FUNCTIONAL MATERIALS
www.afm-journal.de

Diversified Photo/Electronic Functions Based on a Simple Chalcone Skeleton: Effects of Substitution Pattern and Molecular Packing

Xiao Cheng, Zhaoyang Wang, Baolei Tang, Hongyu Zhang, Anjun Qin, Jing Zhi Sun, and Ben Zhong Tang**

Structurally simple chalcone derivatives 1–2 are prepared and their diversified emission behaviors are deeply investigated. Two polymorphs (1G: $\lambda_{em} = 536$ nm, $\Phi_f = 0.08$, $\tau = 1.81$ ns; 1O: $\lambda_{em} = 573$ nm, $\Phi_f = 0.19$, $\tau = 10.82$ ns) with distinctively different emission behaviors are constructed by finely controlling the crystallization conditions of compound 1. 1G exhibits typical amplified spontaneous emission while 1O shows an interesting blue shift under smashing process (1O-S: $\lambda_{em} = 562$ nm, $\Phi_f = 0.23$, $\tau = 6.42$ ns), which is ascribed to their different molecular packing structures and intermolecular interactions. Notably, simply introducing a fluorine substituent effectively endows the crystal with red emission (crystal 2: $\lambda_{em} = 598$ nm, $\Phi_f = 0.16$, $\tau = 18.77$ ns). Thus multicolor emissions including green, yellow, orange, and red emissions are obtained based on this simple chalcone skeleton.

1. Introduction

Organic optoelectronic materials have received intensive interests from both academia and industry for their distinctive advantages of scalable structure and adjustable function.[1] In the history of developing organic optoelectronic materials, a series of basic chromophores came forth and played the role of milestones, such as porphyrin for the artificial photosynthetic system, azo-benzene for the pigments and nonlinear optical materials, and triarylamine for the hole transporting organic semiconductors. Combining different basic fluorophores with various functional groups, plenty of organic functional material systems such as porphyrins, perylene diimides, and quinacridones were designed.[2] For example, modifying the quinacridone framework with electron-withdrawing malononitrile substituents and electron-donating thiophene groups respectively gave acceptor and donor materials in solar cells, while introducing a pentaphenylbenzyl group makes quinacridone a good emitter in organic light-emitting diodes.[3] Meanwhile, based on one single molecule, different properties are also available by modulating the molecular conformation, molecular packing modes and intermolecular interactions or changing the external environment. For example, the electron-transporting *mer*-Alq$_3$ (*mer* = meridional) microcrystals would transform into hole-transporting *fac*-Alq$_3$ (*fac* = facial) microcrystals when heated at 390 °C,[4] and many organic polymorphs also display distinctly different photophysical properties or carrier mobilities.[5] As a typical molecular model of high-potential multifunctional material, tetraphenylethene (TPE) has been well studied in recent years. In addition to the typical aggregation-induced emission (AIE) property, TPE also displays many other profound properties, such as easily tunable emission color, chemo/biosensing, multiple responses under external stimulus.[6] More importantly, it can be used as an effective AIE luminogen (AIE-gen) to transform aggregation-caused quenching (ACQ) fluorophores into AIE materials.[7]

Though lots of functional molecular systems like porphyrin, azo, and TPE were discovered, designed, and expanded, there are many new challenges along with the rapid development of organic optoelectronics. For instance, organic crystals with both high-emission efficiency and high-carrier mobility are still very scarce, and how to design multifunctional organic molecules displaying good photobleaching resistance as well as good diagnosis and treatment functions is always an important problem in materials and medicine areas. Therefore, it is still a significant topic in material science to explore and find novel multifunctional molecular systems. Chalcone, a structurally simple enone, is the central core for the ramification of a variety of important biological-active compounds, and meanwhile it can

---

Dr. X. Cheng, Z. Wang, Prof. J. Z. Sun, Prof. B. Z. Tang
Department of Polymer Science and Engineering
Zhejiang University
Hangzhou 310027, P. R. China
E-mail: sunjz@zju.edu.cn; tangbenz@ust.hk

B. Tang, Prof. H. Zhang
State Key Laboratory of Supramolecular Structure and Materials
College of Chemistry
Jilin University
Qianjin Street, Changchun 130012, P. R. China

Prof. A. Qin, Prof. B. Z. Tang
State Key Laboratory of Luminescent Materials and Devices
South China University of Technology
Guangzhou 510640, P. R. China

Prof. B. Z. Tang
Department of Chemistry
Hong Kong Branch of Chinese National Engineering
Research Center for Tissue Restoration and Reconstruction
The Hong Kong University of Science and Technology
Clear Water Bay, Kowloon, Hong Kong, P. R. China

The ORCID identification number(s) for the author(s) of this article can be found under https://doi.org/10.1002/adfm.201706506.

DOI: 10.1002/adfm.201706506

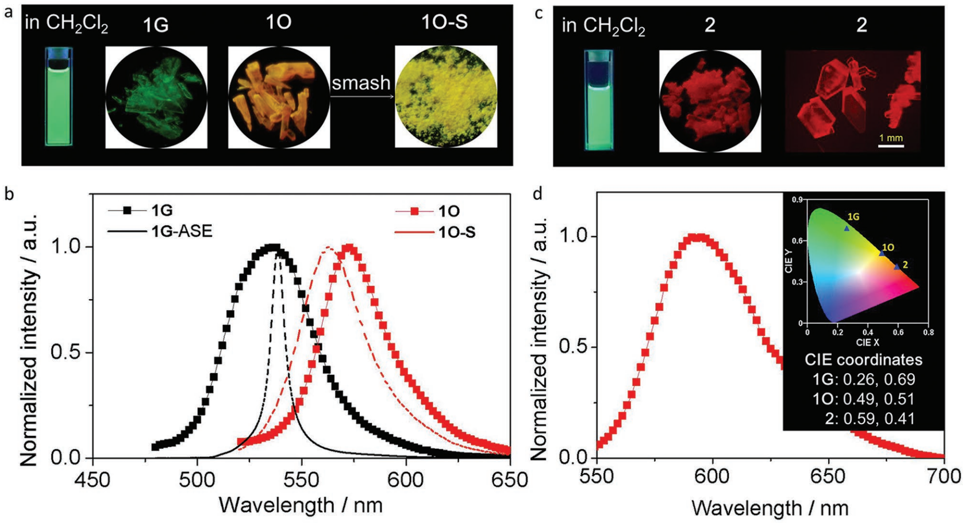

Figure 1. a) Photographs of compound **1** in CH_2Cl_2 solution, **1G**, **1O,** and **1O** after smashing (**1O**-smashed, **1O-S** for short) under UV light. b) PL spectrum, ASE spectrum for **1G** and PL spectra for **1O** and **1O-S.** c) Photographs and microscopy image of compound **2** in solution and crystalline state under UV light. d) PL spectrum of crystal **2** (the inset is the CIE coordinate diagram for crystals **1G**, **1O,** and **2**).

be used as a building block to construct organic luminescent materials.[8] These primary results suggest chalcone derivatives may be a kind of promising multifunctional materials. Investigating their structure–property relationships in depth would be highly conducive to future applications. Following this consideration, we focus on the study of chalcone derivatives, especially the exploration of new compounds, new properties, new functions, and the structure–emission behavior relationship.

In this paper, a series of chalcone derivatives are prepared and they exhibit diversified opto–electronic properties. The relationship between the photophysical properties and electronic/molecular structure and molecular packing mode in solid state have been investigated. The donor–acceptor (D–A) type cyclic chalcone derivative (*E*)-2-(4-(dimethylamino)benzylidene)-1-indanone (**1**)[9] displays polymorph-dependent amplified sponteneous emission (ASE) and its fluoro-substituted analogue **2** displays bright red emission.

2. Results and Discussions

2.1. Synthesis and Crystallization

Compound **1** was reported as a biological-active molecule,[9] but its photophysical property has not been fully investigated yet. It was synthesized according to the literature.[10] At 0 °C, 1.0 g NaOH in 1 mL H_2O was dropwise added to the mixture of 1-indanone (1.32 g, 10 mmol) and 4-(dimethylamino) benzaldehyde (1.49 g, 10 mmol) in 40 mL ethanol. The mixture was stirred for 3 h. The precipitates were filtered out, washed with water and cold ethanol, and then dried as crude product. Compound **1** can form two kinds of crystals in different colors, which are green-colored **1G** and orange-colored **1O**. The crystals were prepared as follows: in a round bottom flask, the crude product was dissolved with CH_2Cl_2 to obtain a concentrated solution and triple amount of hexane was slowly added along the flask-wall without destroying the solution surface. After 12 h at 0–5 °C, plenty of flake-like centimeter-sized crystals precipitated out (named as **1G** for its green color, **Figure 1**a; Figure S1a, Supporting Information), and the structure was characterized by NMR spectroscope. Replacing the CH_2Cl_2/hexane system with polar $CHCl_3$/ethanol system gave rise to amounts of long strip-like orange crystals (named as **1O** for its orange color, Figure 1a; Figure S1b, Supporting Information). ^1H NMR spectrum of **1O** is the same as that of **1G** (Figure S2, Supporting Information), demonstrating that compound **1** displays polymorphism property. Additionally, **1G** phase is easier to prepare compared to **1O**, suggesting that **1G** is a more stable form for compound **1** in solid state. A spontaneous volatilization in different solvents such as CH_2Cl_2 and tetrahydrofuran would always give rise to green emissive solid in **1G** phase, and recrystallization in methanol will also give rise to the **1G** phase.

2.2. Photophysical Properties

Compound **1** exhibits an intense absorption band peaking at 422 nm in CH_2Cl_2 (Figure S3, Supporting Information). Its solution is green emissive (515 nm) with the quantum yield of about 0.17 and a lifetime of 0.90 ns (Figure 1a; Figures S3 and S4, Supporting Information). As the solvent polarity increases, the emission spectra of compound **1** display large red-shift (Figure S3, Supporting Information), according with the D–A (donor–acceptor) property of this type molecule. In toluene, its emission band is centered at 464 nm, while in *N*,*N*-dimethyl formamide, its emission band is peaking at 535 nm. Because of its planar, extended π-conjugated structure, this compound displays ACQ effect in solution. The emission intensity increases and then decreases with the increasing of the solution concentration (Figure S5, Supporting Information). And the emission peak red-shifts by 12 nm. In amorphous solid state, this compound shows very weak fluorescence, while in crystalline state it exhibits different color bright emissions, demonstrating

Table 1. Emission maxima (λ_{em}), quantum yields (Φ_f), fluorescence lifetime (τ_{FL}), radiative rates (k_r), and nonradiative rates (k_{nr}) of crystals **1G**, **1O**, and **2**.

Crystal[a)]	λ_{PL} [nm]	Φ_f [%]	τ_{FL} [ns]	k_r/[s^{-1}]	k_{nr} [s^{-1}]	CIE (x, y)
1G	536	8	1.81	4.4×10^7	5.1×10^8	(0.26, 0.69)
1O	573	19	10.82	1.8×10^7	7.5×10^7	(0.49, 0.51)
2	598	16	18.77	8.5×10^6	4.5×10^7	(0.59, 0.41)

[a)] The radiative rate and nonradiative constants were calculated according to the following relations: $k_r = \Phi_f/\tau_{FL}$; $k_{nr} = (1-\Phi_f)/\tau_{FL}$.

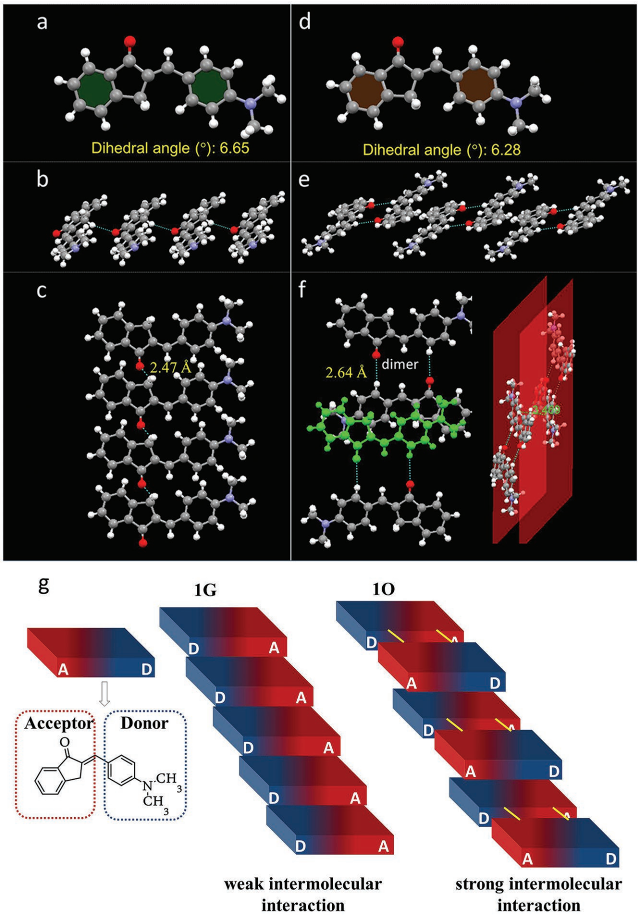

Figure 2. Molecular structures, molecular packing structures, intermolecular interactions among the ordered packing structures of a–c) **1G** and d–f) **1O**, and g) the schematic diagram of the two different packing structures.

this molecule shows crystallization-induced enhanced emission (CIEE) behavior. Two different crystals: the green emissive **1G** and the orange emissive **1O** (Figure 1a), as mentioned earlier, were prepared. Their photophysical properties are summarized in **Table 1**. The **1G** crystal displays typical green fluorescence peaking at 536 nm with a quantum yield of about 0.08 and an average lifetime of 1.81 ns (Figure 1b). Notably, when excited with UV light, **1G** crystal emits brighter fluorescence on the crystal edge than on the body (Figure S1a,b, Supporting Information), indicating self-waveguided emission occurs in the **1G** crystal and thus it may be a possible candidate as organic laser media. **1O** exhibits orange fluorescence peaking at 573 nm, a relatively long-wavelength emission for such structurally simple molecule. The fluorescence quantum yield of **1O** is 0.19, much higher than its **1G** analogue, demonstrating **1O** shows more remarkable CIEE behavior. Consequently, the k_r/k_{nr} ratio (k_r and k_{nr}: radiative rate and nonradiative rate) of **1O** is much higher than that of **1G**. **1O** displays a much longer average lifetime (10.82 ns) compared with **1G** which might result from their different crystal structures (Figure S4, Supporting Information). As shown in Figure S3c in the Supporting Information, the absorption band of **1O** also displays a red shift compared with **1G**, in coincidence with their emission behavior. Additionally, unlike **1G**, **1O** crystal displays bright emission on both its edge and its body (Figure S1c,d, Supporting Information). That is, optical waveguide phenomenon is not available for **1O**.

2.3. Crystal Structures

Both of **1G** and **1O** crystals have high quality and appropriate size for single-crystal X-ray diffraction analysis. The unit cell of **1G** is orthorhombic, belongs to Pca2_1 space group and contains four molecules (Figure S6a, Supporting Information). Each molecule takes a planar conformation with the dihedral angle of 6.65° between the two benzene rings (**Figure 2**a). Each molecule connects its six neighboring molecules by nonclassical intermolecular H-bonds (C—H···O) of 2.47, 2.67 Å and weak C—H···π interactions of 2.72 Å (Figure S6c, Supporting Information). Along crystallographic b axis, a typical step-like packing structure was observed, where molecules are parallel to each other (Figure 2b,c). Consequently, molecules pack into infinite molecular arrays like some waves in the crystallographic bc plane (Figure S6e, Supporting Information). Such ordered packing structure with preferred orientation for a single crystal should be beneficial for the self-waveguided emission.[6] The unit cell of **1O** is monoclinic, belongs to space group C2/c, and contains eight molecules (Figure S6b, Supporting Information). Molecules in **1O** take similar planar conformation as those in **1G**, and the dihedral angle between the two benzene rings is 6.28°, a little smaller than **1G** (Figure 2d). As shown in Figure S6d in the Supporting Information, C—H···O (2.63, 2.64 Å) and C—H···π (2.84, 2.70 Å) interactions were found between the adjacent molecules. Notably, two adjacent molecules with opposite orientations tightly connects with each other by two H-bonds (C—H···O) of 2.64 Å, thus forming a "molecular pair," or to say a special "dimer" (Figure 2e,f). These "dimers" are parallel to each other, and there is nearly no π–π overlap among the "dimers" (Figure 2f). The two molecules of a "dimer" almost lie in one plane, and the distance between the adjacent two "dimers" is about 3.47 Å (Figure 2f). Finally, all these "dimers" pack into infinite 3D staggered space network (Figure S6f, Supporting Information). The different packing structures of the two polymorphs can be depicted as schematic diagram in Figure 2g. Because of the neighboring molecules always take an opposite orientation, there exist relatively strong dipole–dipole interactions among the molecular packing structures in **1O**. Such unique packing structures, including the "dimer" and

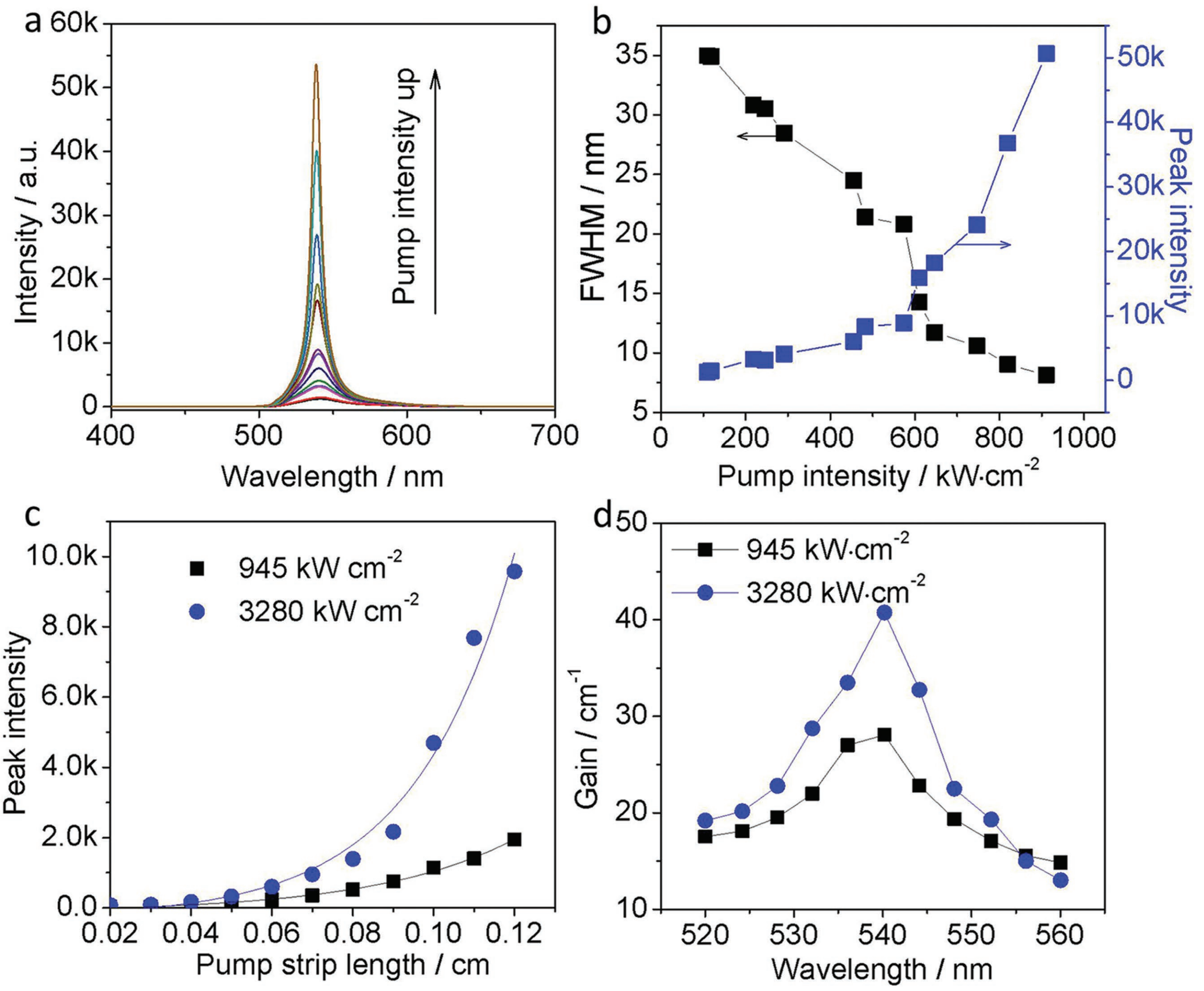

Figure 3. a) PL spectra as a function of the pump laser intensity and b) dependence of the peak intensity and FWHM of emission spectra of crystal **1G**. c) Peak intensity of PL spectra as a function of the pump stripe length and d) the net gain coefficient as a function of wavelength at different pump intensities of crystal **1G**.

the abundant dipole–dipole interactions, endow **1O** with a large red-shifted emission band and a much longer fluorescence lifetime compared with **1G** (Table 1), which is extraordinary for such simple structure.

2.4. ASE of 1G

To test the possibility of **1G** as laser media, ASE measurement was conducted. A slice of **1G** crystal is excited with a pulsed laser beam and the emission spectra are collected from the crystal edge by an optical fiber. The photoluminescent (PL) spectrum of **1G** is normally featured as a broad emission band with the full-width at half-maximum (FWHM) of 48 nm. However, an amplified spontaneous emission is observed when **1G** is excited by laser beam. Upon increasing the laser intensity, the emission bands become narrower with increased intensity. As shown in Figure 1b, the FWHM of the ASE spectra can be reduced to 8.1 nm. **Figure 3**a,b shows the pump intensity-dependent PL spectra as well as the curves of luminescent intensity and FWHM as a function of the pump intensity. The emission intensity increases sharply together with a decreasing FWHM, consistent with the characteristic of ASE. The threshold is less than the initial pump intensity value of 109.3 kW cm^{-2} as the emission spectrum here has been narrowed with a FWHM of 35 nm. The gain coefficients are measured by adjusting a slit. The emission intensity shows an exponential increase as the slit-width increases and higher laser intensity can accelerate the increase of the emission intensity (Figure 3c). The coresponding maximum gain coefficient is 40.7 cm^{-1} (Figure 3d). To verify the propagation direction of the self-waveguided emission light in **1G** crystal, powder X-ray diffraction (PXRD) measurement of some **1G** crystals was conducted. As the single crystals are generally flake-like, most of them would horizontally lie on the substrate surface. Thus some characteristic diffraction planes would be emerged and the crystallographic direction which is perpendicular to the crystal surface can be easily figured out. As shown in Figure S7 in the Supporting Information, the measured sample show several strong diffracion peak corresponding to (200), (400), (800) planes. The calculated distance according to the (200) diffraction peak is 15.05 Å, almost the same as the simulated value (15.01 Å). As the measured sample is a pile of crystals which could not be orderly placed, there are also some crystals which are partially overlapped and their side face is exposed to the X-ray detector. Consequently, the measured sample also show other diffraction signals such as (201), (401), (801) planes.

Although **1O** crystal displays homogeneous emission on edge and body, a single crystal of **1O** was tested with a laser beam and PL spectrum was collected. The FWHM of the PL spectrun collected by a fluorescence spectrometer is generally about 38 nm (Figure 1b). When excited by a high-energy laser beam, **1O** still exhibits a broad emission band with a FWHM of 40 nm, which cannot be narrowed (Figure S8, Supporting Information), indicating that ASE is not available for **1O**. Thus, ASE of organic single crystals has been successfully realized based on this simple molecule, and most importantly, only **1G** phase functions while **1O** not. These results accord well with their characteristics of the different molecular packing structures in crystals and are very important for the understanding of the structure–property relationships for organic luminophores.

2.5. Smashing Effect of 1O

Interestingly, **1O** crystal displays a blue-shift in its emission spectra when the large-sized crystal was smashed into a pile of mini-crystals. The experiment is as follows: A striking force was applied to several **1O** crystal blocks with a small bar such as a spoon handle or a glass rod, these crystal blocks were then shattered into fragments. The emission of the newly generated fracture surface is obviously blue-shifted compared with the previous crystal surface (**Figure 4**a; Figure S1g,h, Supporting Information). A further striking force would smash the fragments into small pieces which we named as **1O-smashed** (**1O-S**) . The previous crystal surfaces were completely destroyed and the presented surfaces were all newly generated fracture surfaces. Thus **1O-S** displays an obvious emission color change from orange to yellow (Figures 1a and 4a), and the emission band blue-shifts to 562 from 575 nm (Figures 1b and 4b). This blue-shift is most likely attributed to the destruction of the intermolecular interactions in the fracture surface as **1O-S** shows identical packing structure with **1O**,[11] which we will analyze in more detail below. As mentioned before, the molecules in the **1O** crystal always come in pairs and show strong dipole–dipole interactions (Figure 2f). Under anisotropic stress like a striking force, the crystals are substantially fragmented and thus those molecules at fracture surface must lose partial intermolecular interactions compared to their "bulk state" when they were still inside. Consequently, the **1O**→**1O-S** can be regarded as a process of decreasing the intermolecular interactions, accompanied with blue shift of the emission (Figure S9, Supporting Information). And the decreased lifetime (6.42 ns) as well as the increased quantum yield (0.23) of **1O-S** also accords well with this process. As shown in Figure 4c, the diffraction peaks of both the as-prepared **1O** and the smashed sample **1O-S** accord well with the single-crystal simulated result, demonstrating that **1O** and **1O-S** belong to the same crystal phase. Thus the smashing process do not destroy the packing structures inside the crystal. However, **1O-S** shows some changes on the PXRD pattern compared with the **1O**. Some new diffraction peaks emerged which were highlighted with some boxes in Figure 4c.

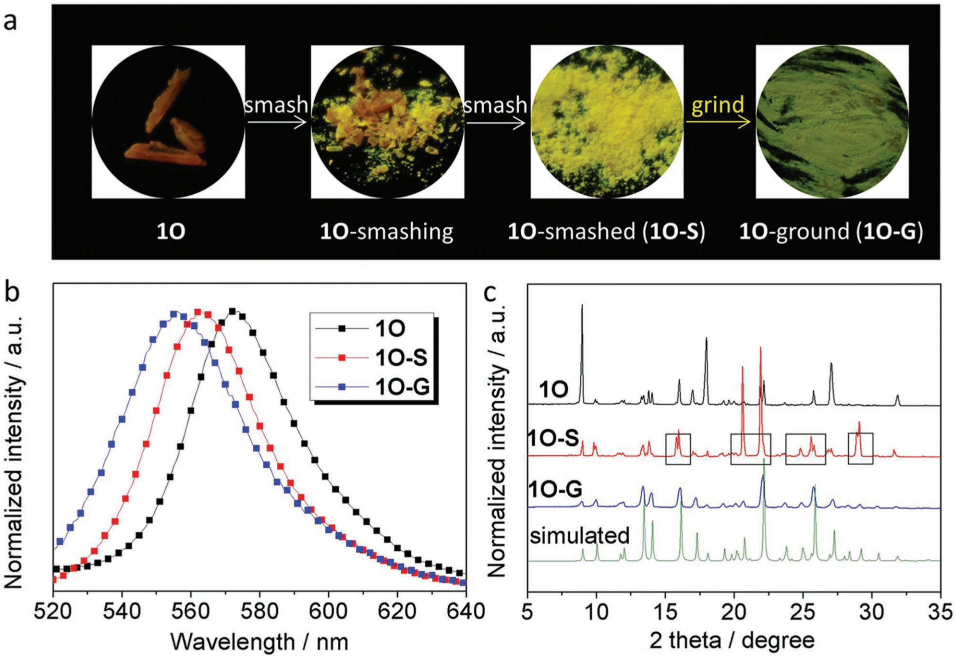

Figure 4. a) The gradual changing photographs under UV light, b) the corresponding blue-shifted PL spectra, and c) PXRD patterns of **1O** when smashed and ground.

This is consisitent with the fact that some new fracture surfaces generate in the smashing process. When ground into powder under a large grinding force for a long time, the sample (named **1O**-ground, **1O-G** for short) still shows strong diffraction peaks, demonstrating the grinding process would further disaggregate the crystal but do not change the crystal form. This differs from those commonly reported compounds which usually become amorphous under grinding process.[12] The emission peak of the ground sample further blue-shifts to 553 nm and the emission color change to green yellow (Figure 4). Compared with **1O** and **1O-S**, the crystal grain size of **1O-G** is small and the morphology is more irregular. As a result, the PXRD peaks of **1O-G** become wider and weaker, and **1O-G** shows a broader emission band with the FWHM of 43.2 nm (FWHMs are 37.8 and 37.4 nm for **1O** and **1O-S**, respectively). Overall, when **1O** is smashed, the newly generated fracture surfaces display an obvious blue-shift, which is most likely assigned to a damage of the originally strong intermolecular interactions. Eventually the smashed sample **1O-S** displays a blue-shifted emission band without changing the spectra shape and FWHM. Correspondingly, its emission color changes from orange to yellow. As this behavior is observed in a smashing process, we call it "smashing effect."

The **1G** crystal shows a different response to smashing treatment. The emission band becomes broader rather than directly blue-shifts without changing the FWHM (Figure S10, Supporting Information). Meanwhile, the emission spectra of the smashed and ground samples are the same. All of these results indicate that **1G** do not exhibit the interesting "smashing effect" as **1O**, which is consisitent with the fact that the intermolecular interactions in **1G** are weaker than those in **1O**. In fact, there were a few fluorophores that displayed large blue-shift when ground, and some of them displaying different responses to different stresses were carefully studied.[11] For example, Yamaguchi and co-workers reported a tetrathiazolylthiophene fluorophore which displayed distinct luminescent responses to anisotropic grinding and isotropic compression.[11b] Wang and co-workers reported a boron diketonate fluorophore which show different mechanoluminescence behavior upon compressing, grinding and smashing.[11c] There are three basic differences between this work and those reported results. First, **1O** shows exceptional crystallizability and it would keep its crystal nature rather than become amorphous even under grinding process, which is useful to research the individual effect of the external force or stress on the crystal luminescence. Second, the gradual changing process were focused on in this work, which is helpful to analyze the relationship among external force, crystal structure and emission behavior more accurately. Third, polymorphs **1O** and **1G** with different crystal structures in this work displays different responses upon smashing, providing more powerful evidence that the interesting "smashing effect" of **1O** results from its special crystal structure.

2.6. Subtle Modification but Large Red-Shift

Highly efficient organic fluorophores with red or near-infrared (NIR) emission have attracted increasing attention for their wide applications in many fields.[13] However, the solid-state brightly emissive red or NIR fluorophores are relatively scarce for their structural complexity and severe fluorescence quenching. Thus designing structurally simple red luminescent materials in solid state is still very important. Compound **1** has a very simple molecular structure and is easy to synthesize. Meanwhile, compound **1** can crystallize into long-wavelength emissive **1O** crystal which displays a large red shift of 58 nm compared with its CH_2Cl_2 solution. These results indicate that this type of cyclic chalcone may be used as a body structure to construct red emissive solid-state organic materials, which is a simple and economical way. In this consideration, we introduced fluorine atom in the molecule and synthesized compound **2**, expecting to get an efficient red fluorophore. The fluorine atom serves two functions. First, its strong electron-withdrawing property will strengthen the D–A character of the moleclue. Second, the fluorine will often form some hydrogen bonds in the solid state, which may enhance the intermolecular interactions and promote the molecules to arrange more closely in the crystal. As expected, large amounts of red crystals with red fluorescence based on compound **2** were obtained (**Figure 5**; Figure S1e,f, Supporting Information). The red emissive crystal phase is a very stable crystal phase for compound **2**, and we cannot obtain another green emissive crystal phase like **1G**. Recrystallization products in different solvents all belong to red emissive crystal phase. Thus crystal **2** means the red crystal in the sections below. It is worth noting that compound **2** is still green emissive in solution but brightly red emissive as crystal (Figure 1c). The absorption and photoluminescence spectra of **2** in solution are almost identical to those of **1** (Figure S11, Supporting Information). The crystals of **2** exhibit an emission band peaking at 598 nm with a quantum yield of 0.16 and a lifetime of 18.77 ns (Figure 1d, Table 1). The CIE (Commission Internationale de L'Eclairage) coordinate is (0.59, 0.41), obviously locating at the red

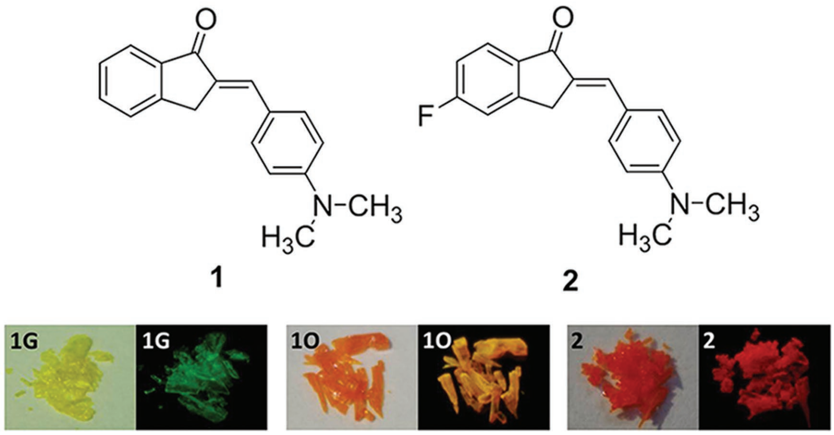

Figure 5. Molecular structures of compounds **1**–**2** and photographs of their crystals under daylight and UV light.

region (Figure 1d). The single crystal structure of **2** is similar with that of **1O**. Molecules pair up as special "dimer" via two C—H···O hydrogen bonds of 2.64 Å, except that one molecule moves toward the dimethylamino terminal of the other molecule (Figure S12a, Supporting Information). Besides the two hydrogen bonds inside the "dimer," there are also some hydrogen bonds of 2.69 Å between the "dimers" (Figure S12, Supporting Information). Additionally, there are strong C—H···F interactions of 2.62 and 2.66 Å among the packing structure (Figure S12b, Supporting Information), which indicates crystal **2** shows stronger molecular interactions compared with crystal **1O**. The combined effect of all these differences in the crystal packing structure and molecular structure facilitates a large red shift for crystal **2**. Consequently, brightly red emissive crystals were fabricated based on a very simple D–A type molecule. As crystal 2 has a similar packing structure with crystal 1O, it also shows continually blue-shifts when smashed and ground (Figure S13, Supporting Information).

3. Conclusion

In conclusion, a series of D–A type cyclic chalcone derivatives were synthesized and they demonstrated plentiful opto–electronic properties, indicating that chalcone is a promising candidate for the construction of advanced opto–electronic materials. Polymorphs **1G** and **1O**, displaying green and orange emission, were prepared. **1G** displays typical ASE behavior while **1O** does not, which is ascribed to their different molecular packing structures. In **1G**, molecules pack into ordered step-like molecular arrays, whereas **1O** shows a special "dimer" packing structure. And there exist relatively strong dipole–dipole interactions among these "dimers" in **1O**. Consequently, **1O** exhibits a largely red-shifted emission band compared with **1G**. Besides, an interesting "smashing effect" was observed for **1O**. When smashed, the emission color of **1O** blue-shifts to yellow. Moreover, simply introducing a fluorine substituent at the para-position relative to the carbonyl group effectively endows the crystal with red emission, as demonstrated by compound **2**. The crystal structures undoubtedly determine the photophysical properties of the polymorphs, as well as whether these crystals display ASE behavior or not. Based on the simple molecular skeleton, multicolor emissions were obtained. We believe these results might not only provide significant information on the topic of the structure–property relationship in material science, but also have good guidance to the research and design of new high-efficiency organic luminophores.

4. Experimental Section

Materials and Instruments: Chemicals of the highest purity level available were obtained from Acros, Sigma-Aldrich, or TCI Chemical Co., and were used without further purification. NMR spectra were recorded on a Bruker Avance 400 or 500 MHz spectrometer with tetramethylsilane as the internal standard, while mass spectra were recorded on a Thermo Fisher ITQ1100 mass spectrometer. Elemental analyses were performed on a FlashEA1112 spectrometer. While UV–vis absorption spectra were recorded on a Shimadzu UV-2550 spectrophotometer, emission spectra were recorded using a Shimadzu RF-5301 PC spectrometer. Absolute fluorescence quantum yields and lifetimes were measured on an Edinburgh FLS920 with or without an integrating sphere. For the laser test, the crystal slices were irradiated by the third harmonic (355 nm) of a Nd:YAG (yttrium–aluminum–garnet) laser at a repetition rate of 10 Hz and pulse duration of about 5 ns. The energy of the pumping laser was adjusted by using the calibrated neutral density filters. The beam was focused into a stripe whose shape was adjusted to 2 × 0.5 mm by using a cylindrical lens and a slit. The edge emission and PL spectra of the crystals was detected using a Maya2000 Pro CCD spectrometer. All measurements were carried out at room temperature under ambient conditions.

(2*E*)-5-Fluoro-2-[[4-(dimethylamino)phenyl]methylene]-2,3-dihydro-1*H*-inden-1-one (**2**). Yield: 73%. ^{1}H NMR (400 MHz, CDCl$_3$): δ 7.88 (dd, J = 9.6 Hz, 5.6 Hz, 1H, Ar H), 7.61 (s, 1H, C=CH), 7.56 (d, J = 9.2 Hz, 2H, Ar H), 7.19 (d, J = 8.2 Hz, 1H, Ar H), 7.10 (td, J = 8.8 Hz, 1.6 Hz, 1H, Ar H), 6.73 (d, J = 8.8 Hz, 2H, Ar H), 3.96 (s, 2H, CH$_2$), 3.05 (s, 6H, CH$_3$). ^{13}C NMR (100 MHz, CDCl$_3$): δ 192.6 (C=O), 167.8, 165.2, 152.1, 151.1, 135.1, 132.8, 129.3, 126.1, 122.8, 115.4, 112.8, 111.8, 40.0, 32.6. ^{19}F NMR (376 MHz, CDCl$_3$): δ -104.14. MS m/z: 281.1 [M]$^+$ (calcd: 281.2). Anal. Calcd (%) for $C_{18}H_{16}FNO$: C, 76.85; H, 5.73; N, 4.98. Found: C, 76.85; H, 5.78; N, 4.89.

Single Crystal X-Ray Diffraction: Single-crystal X-ray diffraction data were collected on a Rigaku RAXIS-PRID diffractometer in ω-scan mode using graphite-monochromated Mo-Kα radiation. Structures were solved with direct methods using the SHELXTL program and refined with full-matrix least squares on F^2. Nonhydrogen atoms were refined anisotropically, while the positions of hydrogen atoms were calculated and refined isotropically.

[CCDC 1575501 for **1G**, 1575502 for **1O**, and 1575503 for **2** contain the supplementary crystallographic data for this paper. These data can be obtained free of charge from The Cambridge Crystallographic Data Centre via www.ccdc.cam.ac.uk/data_request/cif.]

Supporting Information

Supporting Information is available from the Wiley Online Library or from the author.

Acknowledgements

This work was financially supported by the key project of the Ministry of Science and Technology of the People's Republic of China (2013CB834704), the National Natural Science Foundation of China (51573158), and the Innovation and Technology Commission of Hong Kong (ITC-CNERC14S01). A.Q. and B.Z.T. acknowledge the support from the Guangdong Innovative Research Team Program (201101C0105067115).

Conflict of Interest

The authors declare no conflict of interest.

Keywords

amplified spontaneous emission, chalcone, crystallization-induced enhanced emission, mechanochromism, red emitting

Received: November 8, 2017
Revised: December 14, 2017

[1] a) D. Li, H. Zhang, Y. Wang, *Chem. Soc. Rev.* **2013**, *42*, 8416; b) M. Y. Wong, E. Zysman-Colman, *Adv. Mater.* **2017**, *29*, 1605444; c) C. Li, J. Wei, J. Han, Z. Li, X. Song, Z. Zhang, J. Zhang, Y. Wang, *J. Mater. Chem. C* **2016**, *4*, 10120; d) H. Kobayashi, P. L. Choyke, *Acc. Chem. Res.* **2011**, *44*, 83; e) J. Qian, Z. Zhu, A. Qin, W. Qin, L. Chu, F. Cai, H. Zhang, Q. Wu, R. Hu, B. Z. Tang, S. He, *Adv. Mater.* **2015**, *27*, 2332; f) X. Shi, C. Y. Y. Yu, H. Su, R. T. K. Kwok, M. Jiang, Z. He, J. W. Y. Lam, B. Z. Tang, *Chem. Sci.* **2017**, *8*, 7014; g) M. Tian, Y. Liu, Y. Sun, R. Zhang, R. Feng, G. Zhang, L. Guo, X. Li, X. Yu, J. Z. Sun, X. He, *Biomaterials* **2017**, *120*, 46; h) D. Li, J. Yu, *Small* **2016**, *12*, 6478; i) J. Mei, Y. Hong, J. W. Y. Lam, A. Qin, Y. Tang, B. Z. Tang, *Adv. Mater.* **2014**, *26*, 5429; j) W. Zhang, J. Yao, Y. S. Zhao, *Acc. Chem. Res.* **2016**, *49*, 1691; k) H. Dong, C. Zhang, Y. S. Zhao, *J. Mater. Chem. C* **2017**, *5*, 5600; l) H. He, E. Ma, Y. Cui, J. Yu, Y. Yang, T. Song, C.-D. Wu, X. Chen, B. Chen, G. Qian, *Nat. Commun.* **2016**, *7*, 11087.

[2] a) C. Borek, K. Hanson, P. I. Djurovich, M. E. Thompson, K. Aznavour, R. Bau, Y. Sun, S. R. Forrest, J. Brooks, L. Michalski, J. Brown, *Angew. Chem., Int. Ed.* **2007**, *46*, 1109; b) M. Sun, K. Müllen, M. Yin, *Chem. Soc. Rev.* **2016**, *45*, 1513; c) C. Wang, Z. Zhang, Y. Wang, *J. Mater. Chem. C* **2016**, *4*, 9918; d) S. Wan, Z. Ma, C. Chen, F. Li, F. Wang, X. Jia, W. Yang, M. Yin, *Adv. Funct. Mater.* **2016**, *26*, 353; e) S. Mo, Q. Meng, S. Wan, Z. Su, H. Yan, B. Z. Tang, M. Yin, *Adv. Funct. Mater.* **2017**, *27*, 1701210.

[3] a) J. J.-A. Chen, T. L. Chen, B. Kim, D. A. Poulsen, J. L. Mynar, J. M. J. Fréchet, B. Ma, *ACS Appl. Mater. Interfaces* **2010**, *2*, 2679; b) T. Zhou, T. Jia, B. Kang, F. Li, M. Fahlman, Y. Wang, *Adv. Energy Mater.* **2011**, *1*, 431; c) C. Wang, K. Wang, Q. Fu, J. Zhang, D. Ma, Y. Wang, *J. Mater. Chem. C* **2013**, *1*, 410.

[4] H. Bi, H. Zhang, Y. Zhang, H. Gao, Z. Su, Y. Wang, *Adv. Mater* **2010**, *22*, 1631;

[5] a) L. Yu, *Acc. Chem. Res.* **2010**, *43*, 1257; b) T. He, M. Stolte, C. Burschka, N. H. Hansen, T. Musiol, D. Kälblein, J. Pflaum, X. Tao, J. Brill, F. Würthner, *Nat. Commun.* **2015**, *6*, 5954; c) A. M. Hiszpanski, R. M. Baur, B. Kim, N. J. Tremblay, C. Nuckolls, A. R. Woll, Y.-L. Loo, *J. Am. Chem. Soc.* **2014**, *136*, 15749.

[6] a) J. Mei, N. L. C. Leung, R. T. K. Kwok, J. W. Y. Lam, B. Z. Tang, *Chem. Rev.* **2015**, *115*, 11718; b) J. Mei, Y. Hong, J. W. Y. Lam, A. Qin, Y. Tang, B. Z. Tang, *Adv. Mater.* **2014**, *26*, 5429.

[7] Z. Zhao, J. W. Y. Lam, B. Z. Tang, *J. Mater. Chem.* **2012**, *22*, 23726.

[8] a) X. Cheng, Y. Zhang, S. Han, F. Li, H. Zhang, Y. Wang, *Chem. Eur. J.* **2016**, *22*, 4899; b) X. Cheng, K. Wang, S. Huang, H. Zhang, H. Zhang, Y. Wang, *Angew. Chem., Int. Ed.* **2015**, *54*, 8369; c) L. Wang, Z. Zhang, X. Cheng, K. Ye, F. Li, Y. Wang, H. Zhang, *J. Mater. Chem. C* **2015**, *3*, 499; d) X. Wang, Z.-Z. Li, S.-F. Li, H. Li, J. Chen, Y. Wu, H. Fu, *Adv. Opt. Mater.* **2017**, *5*, 1700027; e) L. Varinska, M. Wijhe, M. Belleri, S. Mitola, P. Perjesi, M. Presta, P. Koolwijk, L. Ivanova, J. Mojzis, *Eur. J. Pharmacol.* **2012**, *691*, 125.

[9] a) P. Perjési, *Monatsh. Chem.* **2015**, *146*, 1275; b) J. Vašková, R. Reisch, L. Vaško, M. Poškrobová, I. Kron, J. Guzy, P. Perjési, *In Vitro Cell. Dev. Biol.: Anim.* **2013**, *49*, 354.

[10] T. M. Kadayat, C. Park, K.-Y. Jun, T. B. T. Magar, G. Bist, H. Y. Yoo, Y. Kwon, E.-S. Lee, *Bioorg. Med. Chem.* **2015**, *23*, 160.

[11] a) J. Wu, Y. Cheng, J. Lan, D. Wu, S. Qian, L. Yan, Z. He, X. Li, K. Wang, B. Zou, J. You, *J. Am. Chem. Soc.* **2016**, *138*, 12803; b) K. Nagura, S. Saito, H. Yusa, H. Yamawaki, H. Fujihisa, H. Sato, Y. Shimoikeda, S. Yamaguchi, *J. Am. Chem. Soc.* **2013**, *135*, 10322; c) L. Wang, K. Wang, B. Zou, K. Ye, H. Zhang, Y. Wang, *Adv. Mater.* **2015**, *27*, 2918.

[12] a) Y. Gong, G. Chen, Q. Peng, W. Z. Yuan, Y. Xie, Sh. Li, Y. Zhang, B. Z. Tang, *Adv. Mater.* **2015**, *27*, 6195; b) W. Z. Yuan, Y. Tan, Y. Gong, P. Lu, J. W. Y. Lam, X. Y. Shen, C. Feng, H. H-Y. Sung, Y. Lu, I. D. Williams, J. Z. Sun, Y. Zhang, B. Z. Tang, *Adv. Mater.* **2013**, *25*, 2837.

[13] a) M. Shimizu, R. Kaki, Y. Takeda, T. Hiyama, N. Nagai, H. Yamagishi, H. Furutani, *Angew. Chem., Int. Ed.* **2012**, *51*, 4095; b) N. Karton-Lifshin, L. Albertazzi, M. Bendikov, P. S. Baran, D. Shabat, *J. Am. Chem. Soc.* **2012**, *134*, 20412; c) H. Lu, Y. Zheng, X. Zhao, L. Wang, S. Ma, X. Han, B. Xu, W. Tian, H. Gao, *Angew. Chem., Int. Ed.* **2016**, *55*, 155.